# Site of Tagging Influences the Ochratoxin Recognition by Peptide NFO4: A Molecular Dynamics Study

Aby A. Thyparambil, Tigran M. Abramyan, Ingrid Bazin, Anthony Guiseppi-Elie

# Site of Tagging Influences the Ochratoxin Recognition by Peptide NFO4: A Molecular Dynamics Study

Aby A. Thyparambil[a,b], Tigran M. Abramyan[c], Ingrid Bazin[d] and Anthony Guiseppi Elie[a,b,d,e,*].

[a] Center for Bioelectronics, Biosensors and Biochips (C3B), Texas A&M University, College Station, TX 77843, USA

[b] Department of Biomedical Engineering, College of Engineering, Texas A&M University, College Station, TX 77843, USA

[c] Computational Biophysics & Molecular Design, Center for Integrative Chemical Biology and Drug Discovery, Eshelman School of Pharmacy, University of North Carolina, Chapel Hill, NC 27599-7363, USA

[d] Ecole des mines d'Ales, institut Mines Telecom, 6 avenue de Clavieres, 30319 Ales cede, France

[e] ABTECH Scientific, Inc., Biotechnology Research Park, 800 East Leigh Street, Richmond, VA 23219, USA

*KEYWORDS. Peptides, Hapten, Ochratoxins, Affinity Tag, Binding Energy, Bias Exchange Metadynamics, Markov State Models, All-Atom Molecular Dynamics.*

**ABSTRACT:** Molecular recognition by synthetic peptides is growing in importance in the design of biosensing elements used in the detection and monitoring of a wide variety of hapten bioanlaytes. Conferring specificity via bio-immobilization and subsequent recovery and purification of such sensing elements are aided by the use of affinity tags. However, the tag and its site of placement can potentially compromise the hapten recognition capabilities of the peptide, necessitating a detailed experimental characterization and optimization of the tagged molecular recognition entity. The objective of this study was to assess the impact of site-specific tags on a native peptide's fold and hapten recognition capabilities using advanced molecular dynamics (MD) simulation approach involving bias exchange metadynamics and Markov state models. The *in-solution* binding preferences of affinity tagged NFO4 (VYMNRKYYKCCK) to chlorinated (OTA) and non-chlorinated (OTB) analogues of ochratoxin were evaluated by appending hexa-histidine tags (6× His-tag) to the peptide's N-terminus (NterNFO4) or C-terminus (CterNFO4), respectively. The untagged NFO4 (NFO4), previously shown to bind with high affinity and selectivity to OTA, served as the control. Results indicate that the addition of site-specific 6× His-tags altered the peptide's native fold and the ochratoxin binding mechanism, with the influence of site-specific affinity tags being most evident on the peptide's interaction with OTA. The tags at the N-terminus of NFO4 preserved the native fold and actively contributed to the non-bonded interactions with OTA. In contrast, the tags at the C-terminus of NFO4 altered the native fold and were agnostic in its non-bonded interactions with OTA. The tags also increased the penalty associated with desolvating the peptide-OTA complex. Interestingly, the tags did not significantly influence the non-bonded interactions or the penalty associated with solvating the peptide-OTB complex. Overall, the combined contributions of non-bonded interaction and solvation penalty were responsible for the retention of the native hapten recognition capabilities in NterNFO4 and compromised native recognition capabilities in CterNFO4. Advanced MD approaches thus provide structural and energetic insights critical to evaluate the impact of site-specific tags, and may aid in the selection and optimization of the binding preferences of a specific biosensing element.

## INTRODUCTION

A major percentage of the pesticides, herbicides, toxins, metals and allergens for which there is need to design and fabricate biosensors are potential haptens.[1] Haptens are a class of low molecular weight chemicals that are inherently not antigenic but can elicit an immune response when conjugated to serum proteins or low molecular weight peptides.[1] Prolonged exposures to some haptens have been linked to multiple health risks including organ failure, increased cancer risk, genotoxicity, autoimmune disorders, and hypersensitive reactions.[2-4] During the last decade a wide range of sensing and detection platforms involving the use of synthetic peptides have been developed against a variety of haptens such as ochratoxin-A (OTA), 2, 4, 6 trinitrotoluene, and 2,4 dichlorophenoxyacetic acid.[5-10] In all these applications, site-specific conjugation of the molecular recognition peptide to achieve its immobilization on or within the biosensing element or bioassay was enabled by the use of site-specific affinity tags. The tags of the conjugates were essential to ensure the immobilization, efficient hapten recognition, recovery, stability, and cost-effective operation of the detection platform. In this regard, affinity tags are a very popular type of tag as they allow for orientation of the recognition peptide and possible reusability of the biotransducer platform.[11, 12]

The introduction of affinity tags generally involves the covalent conjugation of contiguous amino acids, peptides, enzymes, and protein domains to specific sites of the molecular recognition entity. These tags then bind with high specificity to a target biological or a chemical ligands on the adsorbent phase, In so doing the tag facilitates the immobilization of the

molecular recognition entity on the detection platform while optimally orienting it towards the solution phase for hapten capture.[13] Furthermore, immobilization aids in the cost-effective usage of the molecular recognition platforms, by facilitating the recovery, stability, and possible reusability of the detection platform from the bioanalyte matrix. However, a major challenge in the design of biosensing elements pertains to the selection and location of affinity tags, so as not to compromise the inherent activity, specificity, and selectivity of the molecular recognition entity. Ideally, affinity tags are expected to be small in size to prevent or minimize direct interaction with the biosensing elements or with the analyte of interest. Direct interactions of tags with the biorecognition peptide can also affect the orientation and the molecular recognition properties of the sensing element. Tagging the molecular recognition entity is particularly more challenging when the tags and sensing elements are of comparable size and chemistry.

Hexahistidine tag (6×His-tag) is one such example of an affinity tag that binds with high affinity to substrates coated with metal ions, specifically zinc.[8, 14] Because of its short length and relative ease of synthesis and removal, 6×His-tags are widely used in protein purification and immobilization.[15-17] The introduction of 6×His-tag may have either positive or negative effects on the biochemical properties of a molecular recognition entity of a sensing element.[7, 8, 18-22] For example, the addition of 6×His-tags has been found to increase the sensitivity of binding assays with tagged ScFv.[23] But, in case of glycine N-acyltransferase GNAT peptides from *Pseudomonas aeruginosa*, the 6×His-tags were found to act as weak competitive inhibitors and interfered with the intrinsic activity of the peptide.[22] In addition to the type of tag, the site of tag conjugation may also affect the intrinsic biochemical activity of the molecular recognition entity of a sensing element.[18] For example, drugs conjugated to antibodies via glutamine tags showed differences in their pharmacokinetics depending on the location of the drug on the heavy and light chains of the antibodies.[24] Similarly, on solid platforms, a synthetic peptide (12 amino acid long) oriented with 6× His-tag on the N-terminus was found to be significantly better at hapten recognition than those oriented with the affinity tags on the C-terminus of the peptide.[7, 8] Clearly, the impact of site-specific tags on the biological recognition capabilities of sensing elements is non-trivial, especially when the tags are of comparable size and chemistry and must be thoroughly assessed before being reliably applied for biosensing applications.

One approach to identifying a site-specific tag suitable for peptide immobilization involves cyclic testing of known tags at different sites using routine experimental biophysical techniques, such as equilibration dialysis[25, 26] or surface plasmon resonance.[27, 28] Unfortunately, these techniques lack the resolution of sub-molecular events and the likelihood of such an approach leading to an optimized design is extremely small. A sub-molecular understanding of the impact of tags on the peptide-hapten binding is essential because of the dynamic nature of the peptide. At equilibrium, peptides exist in an ensemble of conformational states with their respective probabilities.[29-32] Within this ensemble of peptide conformations, haptens bind with high affinity to conformations that produce the bound state of the peptide, while weakly interacting hapten-peptide pairs are associated with other conformational states. It is important to note that this may not be a single confor mation but in fact a smearing of energetically similar confor mations or an alternate minimum. Consequently, haptens that bind to the peptides with high affinity tend to shift the popula tion distribution favoring the bound states of the peptide hapten complex; and haptens that bind to the peptides with low affinity tend to skew the equilibrium towards the unbound states.[31, 33] The foregoing requires that a clear energetic distinction be established between bound and unbound states. In essence, the impact of tags on a peptide's hapten binding properties, including its affinity, specificity and selectivity, can be thoroughly assessed, or even engineered, by considering the population distribution and redistribution of a peptide's conformational states, in tandem with the structure-energetic characteristics of the bound states. Undoubtedly, *in silico* techniques like molecular dynamics (MD) are the best tools for visualizing such sub-molecular events.

However, regular molecular dynamics (MD) approaches alone are inept in generating thermodynamically favored conformations of peptide-hapten complexes or in describing the kinetics of peptide-hapten binding.[30, 33] Regular MD simulations typically capture biophysical phenomena occurring on the order of hundreds of nanoseconds, while the unbinding kinetics of a peptide-hapten system with high affinity would involve time scales often exceeding several hours. As an alternative, the authors have recently demonstrated the capabilities of advanced MD simulations involving accelerated configurational search and Markov state models (MSM) to assess the mechanism involved in the binding of synthetic peptides to a hapten such as ochratoxin.[34]

The objective of the current study was to assess the impact of dimensionally and chemically comparable site-specific tags on a peptide's fold and hapten recognition. For this purpose, the impact of 6× His-tag and its site of placement on the native fold of NFO4 and its native in-solution binding behavior were assessed using an *in silico* approach involving enhanced MD sampling in conjunction with MSM. NFO4, a dodecamer (VYMNRKYYKCCK), was previously shown to bind with high affinity and selectivity to the chlorinated analogue (OTA) of a hapten like ochratoxin as opposed to a non-chlorinated analogue (OTB) (Figure 1).[6, 34, 35] The affinity tags were "covalently conjugated" via peptide bond formation to the N-terminus (NterNFO4) and C-terminus (CterNFO4) of the peptide. Untagged NFO4 served as the control. All binding energy calculations were carried out in explicit solvent with the solution pH mimicking wine (pH 3-4), a matrix of concern for the presence of ochratoxins. Advanced sampling was performed using bias-exchange metadynamics (BEMD), which involves the introduction of time dependent bias potentials to sample rare events and generate experimentally relevant biomolecular conformations.[36] The equilibrium dynamics of the system was then predicted based on the conditional transition probability of diverse peptide conformations using MSM functionalities provided within HTMD.[37]

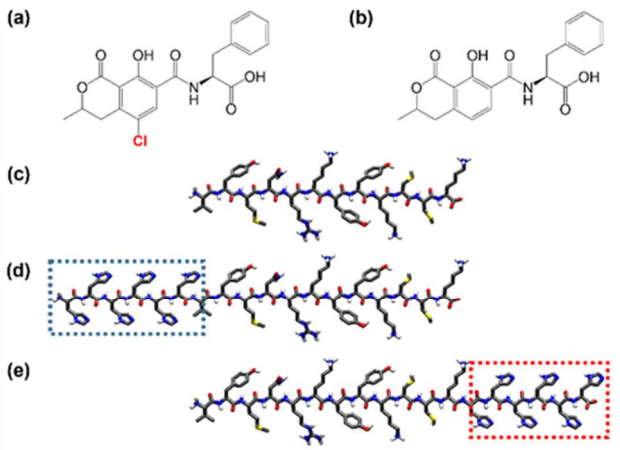


**Figure 1:** Chemical structure of (a) ochratoxin-A (OTA), (b) ochratoxin-B (OTB), (c) the dodecapeptide NFO4, (d) NterNFO4 and (e) CterNFO4. The structural analogues of ochratoxins (i.e. OTA and OTB) differ in the 'Cl' moiety highlighted in red. Similarly, the peptides differ in the location of 6× His-tags with the NFO4 lacking a tag, NterNFO4 having a tag at the N-terminus of NFO4 (blue dotted box), and CterNFO4 having a tag at the C-terminus of NFO4 (red dotted box).

## ▪ EXPERIMENTAL PROCEDURES

**Model Setup:** Linear structures of VYMNRKYYKCCK (NFO4), HHHHHH-VYMNRKYYKCCK (NterNFO4) and VYMNR KYYKCCK-HHHHHH (CterNFO4) were generated from the primary sequence of the respective peptides using Visual Molecular Dynamics (v 1.9.2).[38] The initial coordinates of ochratoxins (OTA and OTB) were obtained from the ZINC database; and the topology and parameters for the ochratoxins were generated through the automated topology builder (ATB) and repository 2.1.[39, 40] The amino acids and the hapten were modeled with the likely protonation state in a wine-like matrix of pH 3-4. Consequently, the N-termini, histidines, arginines, and lysines within the peptide were protonated, and the C-termini, aspartic and glutamic acids, and the ochratoxins were modeled as uncharged or neutral.

The simulation procedure was previously described in detail.[34] Briefly, MD simulations were carried out in a GROMACS (v 5.0.4) simulator.[41] GROMOS 54A7 force field and SPC water model was used to describe the molecular mechanics of the modelled system.[42, 43] Long-range electrostatic interactions (real-space truncation at 1.4 nm and grid spacing of 0.12 nm) was handled using periodic boundary conditions with particle mesh Ewald summation, and was updated every 10 fs, together with the pair list generation. The Lennard–Jones 6–12 potential was used to evaluate the van der Waals interactions within a cutoff distance of 1.4 nm and was updated at every step. The LINCS algorithm was used to constrain the lengths of covalent bonds and the geometry of the water molecules. A coupling scheme using velocity rescaling with a stochastic term was applied to maintain the temperature at 298 K with the modified Berendsen coupling method and a relaxation time constant of 0.1 ps. The pressure of the system was maintained at 1 bar using Parrinello-Rahman coupling method with a time step of 2 fs and a relaxation time constant of 2.0 ps. The starting atomic velocities were generated randomly using Maxwell–Boltzmann distribution at 298 K.

**Sampling of Kinetically Relevant Peptide and Peptide-Hapten Configurations**. Prior to binding simulations, the peptide configurations were sampled using BEMD.[44, 45] All BEMD simulations were performed in the NPT ensemble at 298K and 1 bar using GROMACS (v 5.0.4) compiled with the PLUMED (v 2.2.2) plugin.[46] Three independent BEMD simulations were initialized from random configurations of the peptide. For each BEMD simulation of peptide folding, three replicas were used. Each of the first two replicas was biased by a different collective variable (CV), namely, main chain radius of gyration ($R_g$), and number of hydrogen bonds ($N_{hb}$) within the peptide main chain. The third replica was simulated without any bias. From the peptide folding simulations, four macrostates were identified and were used in the binding simulations. For each of the sampled peptide configurations, binding simulation was initiated by biasing five different CVs. The first four replicas were biased by main chain $R_g$, $N_{hb}$ between the peptide and haptens, degree of similarity between the torsional angles traversed by the peptide and hapten ($\Phi_{corr}$), and the distance between the center of mass of the hapten and center of mass of the peptide ($d_1$). The fifth replica was simulated without any bias.

The convergence and equilibrium state of the BEMD trajectories were verified by calculating the potential of mean force (PMF) along different CVs (Figure S1). The evolution of each replica in the free energy landscape was further monitored and traced using the replica index. For the peptide folding and binding simulations, all CVs could reconstruct similar PMF profile. However, there were differences in the convergence time. In general, the simulation using CVs such as $R_g$, $N_{hb}$, and $d_1$ reached convergence in relatively similar simulation time (<30 ns). PMF took longer to converge (>40 ns) when biased along $\Phi_{cor}$. When all four CVs were used, the average replica exchange probability was ~0.26. After equilibration and convergence, the simulations were extended for an additional 100 ns.

**MSM Construction for Predicting Folded Conformations and Binding Kinetics.** MSM construction, analysis and validation were achieved using the functionalities provided with HTMD (v 1.7.0).[37, 47, 48] It should be pointed out that the main goal of the application of the MSM analysis in the current study was to obtain the population distribution of the macrostates of each molecular system rather than the transition rates among these macrostates. Also, the terminology 'macrostates' was adopted from the HTMD documentation to indicate the metastable states of the peptide. Distinct folded conformations of the peptide were identified from MSM by featurizing the intramolecular contacts made by the alpha carbon atoms of the peptide. For the binding simulations, all the distances between the heavy atoms of the hapten and the peptide were used as the metric to resolve the conformational space. For the current study, the unbiased replica from three independent simulations was used for the MSM model construction .Two atoms were in contact if their distance was less than 5 Å. Time-lag independent component analysis (IC) was performed on the featurized trajectories to find the slow linear sub-space of the input features. IC components that accounted

for > 90% of the total kinetic variance in the configurations were retained for projection and analysis. For binding simulations, dimensionality reduction was achieved by projecting the IC components onto five dimensions. Each IC component was subsequently scaled according to its corresponding eigenvalue to obtain a kinetic map in which Euclidean distances were proportional to kinetic distances, providing an optimal space to perform clustering. Mini batch k-means clustering method was employed to obtain 100 microstates.

Markov model was constructed by the analysis of the implied time scales (ITS) (Figure S2). The validity of the Markov model was verified using Chapman–Kolmogorov. The robustness of MSM was also assessed by increasing the number of clusters and projected dimensions. The number of macrostates was determined by the separation of the transitions in the ITS plot. Macrostates were identified by lumping kinetically close microstates using the Perron cluster cluster analysis (PCCA+) lumping algorithm. For each macrostate, the binding free energy (equation 1) and the equilibrium distribution of the peptides were computed from the reversible transition matrix by comparing the probabilities of bound to unbound states. The reversible transition matrix was estimated using the maximum likelihood estimator. The binding free energies of the peptide-hapten complex at equilibrium were calculated with the following equation

$$\Delta G^{\circ}_{binding} = -kT \ln\left(\frac{p_{bound}}{p_{unbound}}\right), \qquad (1)$$

where $p_{\text{bound}}$ is the equilibrium probability of the complex in the bound state, $p_{\text{unbound}}$ is the equilibrium probability of the unbound state of the complex with no peptide-hapten contacts.

**Trajectory Analysis.** Trajectories were visualized using Visual Molecular Dynamics (VMD v 1.9.8). Analysis tools provided with GROMACS were used for estimating the radial distribution function of water (RDF) around the peptide and the hapten, root-mean-squared fluctuation (RMSF), the H-bond profile, and for generating the contact maps.[41] DSSP analysis provided with MDtraj (v 1.7.2.) was used for secondary structure analysis.[49]

The binding free energy of the individual macrostate was further decomposed as a cumulative sum of three main energetic components: non-bonded energetic contributions, solvation penalty, and conformational entropy. The non-bonded energetic contributions and solvation penalties of the peptide-hapten complex (associated with solvating the polar and non-polar groups within the bound complex) were estimated using g_mmpbsa, a GROMACS-based plugin for high-throughput MM/PBSA calculation.[50] Penalties involved in conformational entropy were obtained by quasi-harmonic mode analysis, using the functionalities provided in GROMACS.

## ▪ RESULTS AND DISCUSSION

**Site-Specific 6× His Tag Influence NFO4 Folding**. BEMD was applied to fully explore the conformational space of NFO4 to identify the conformations relevant to hapten binding. For this purpose, all simulations were initiated from fully extended conformations of the peptides, and were carure S1). To assure equilibrium, the simulations were extended for an additional 100 ns. Once the peptide conformations were sampled, the lowest energy conformations were identified using MSM. Figure 2 represents the free energy surface (FES) and the population distribution of each conformation following the projection of the two major IC components (represented by IC1 and IC2). Within the FES, the four low free energy basins were designated as '1', '2', '3', and '4' and the equilibrium distribution of each of these peptide conformations were also provided. The peptide structure that was representative of each basin is shown in the adjacent panel. Table 1 summarizes the structural and energetic attributes of these four macrostates of the peptides. Figures S3–S6 provide information on the RMSF, secondary structure preference, contact map, and the average number of intramolecular H bonds for each state of the peptides, respectively. In general, discussion will be limited to the peptide conformation represented by basin '4', the dominant conformation in each of the peptide system.

**(a) NFO4:** Structural characteristics of the most dominant conformation in NFO4 (NFO4 '4', 99%, Figure 2a) indicated a bent structure, with the constituent residues being rigidly held (RMSF < 0.2 nm) (Figure S3a). In the bent structure, 1 4 formed the trailing segment, residues 5 8 formed the loop structure and residues 9 12 formed the leading seg ment of the peptide. At least 4 of the 12 residues (Met3, Asn4, Lys8 and Cys9) within the bent were involved in intramolecu lar H bonding (Figure S4a). Secondary structure analysis of the sampled NFO4 conformations indicated a general prefer ence towards β turn (33%) and coiled like (67 %) structures. The proximity of the neighboring residues and the potential intramolecular contacts might be responsible for the reduced flexibility of the residues (Figure S5a). Overall, the folded conformation of the peptide was relatively stable compared to its unfolded conformation by 4.5 $k_bT$.

**(b) NterNFO4**: Of the 18 residues in NterNFO4, residues 1 6 represent, the 6× His tag appended to the N terminus, and residues 7 18 represent the NFO4 peptide. Within the dominant peptide population (NterNFO4 '4', 99%, Figure 2b), residues 1 5 were flexible (RMSF > 0.3 nm) and unstructured while the remaining residues were involved in a compact bent structure formation that was relatively less flexible than the N terminus end of the peptide (Figure S3b and S4b.). In the bent structure, the trailing and the leading segments in the β-turn were composed of residues 6-10 and residues 13-18 respectively. The residues 11-12 formed the peptide's loop. The proximity of several residues (distance < 0.5 nm, Figure S5b), especially within the bent structure resulted in at least 9 intramolecular H-bonds between Val7, Tyr8, Met9, Asn10, Tyr13, Tyr14, Lys15 and Cys10. The peptide's structures were additionally stabilized by H-bonding with the solvent (Figure S6b). Overall, the introduction of 6× His-tags at the N-termini of NFO4 preserved the native peptide fold and did not shift its overall stability (<0.5 $k_bT$), despite altering some of the intrinsic contact network within the native NFO4 peptide.

**(c) CterNFO4**: CterNFO4 represented C-termini modified NFO4 with residues 1-12 representing the native NFO4 pep-

tide and residues 13-18 representing the 6× His-tag appended to the C-terminus of the peptide. Unlike NFO4 and NterNFO4, CterNFO4 favored a broader distribution of the peptide conformations (Figure 2c)). With the C-terminus tag in place many of the peptide segments were too far apart (> 0.5 nm) to make intra-molecular contacts. The drop in ordered structure was an additional indicator of the disruptive influence of 6× His-tags on the intrinsic contact network of NFO4. The disruption in the contact network also explains the peptides' enhanced flexibility (> 0.6 nm) (Figure S3c). Interestingly, the dominant conformation of CterNFO4 was relatively more stable (> 1.0 $k_bT$) than NFO4 and NterNFO4 and favored ordered structure, with 17% β-turn and 83% coil. This is an interesting dichotomy, a broader distribution of states but with the dominant state being more stable. Overall, the addition of 6× His tag at the C termini of NFO4 reduced the secondary structure content, disrupted the native contacts and increased the residue flexibility, all of which compromised the native fold.

The combined assessment of the above results suggests that the site specific placement of the affinity tags can affect the native fold of the NFO4 peptide. While 6× His tags at the N terminus of NFO4 showed a general tendency to preserve the native peptide fold, the tags at the C terminus of the NFO4 had a disruptive influence on the peptide's native fold.

**Table 1: Structural and Energetic Preferences of the Folded Peptides**

| Recognition Molecule | Number of Residues[1] | Pref. Macro.[2] | Basin Depth[3] | Secondary Structure Preference[4] | Pr.-Pr. H-bonds[5] | Pr.-Solv. H-bonds[6] |
|---|---|---|---|---|---|---|
| NFO4 | 12 | '4' | 4.5 $k_bT$ | 33% β-turn, 67 % Coil | 4 | 38 |
| NterNFO4 | 18 | '4' | 4.7 $k_bT$ | 44% β-turn, 56 % Coil | 9 | 58 |
| CterNFO4 | 18 | '4' | 5.4 $k_bT$ | 17% β-turn, 83% Coil | 8 | 60 |

[1] Number of Residues refers to the total number of amino acids constituting the peptide.
[2] Pref. Macro. refers to the preferred macrostate which was most populated at equilibrium as determined by the MSM analysis..
[3] Basin depths refer to the free energy associated with the most preferred model, as determined from the MSM analysis.
[4] Secondary structure preference refers to the average secondary structure content of the most preferred model.
[5] Pr.-Pr. H-bonds refer to the average number of peptide-peptide hydrogen bonds (H-bonds) within the most preferred macrostate.
[6] Pr.-Solv. H-bonds refer to the average number of hydrogen bonds (H-bonds) between the peptide and the solvent within the most preferred macrostate.

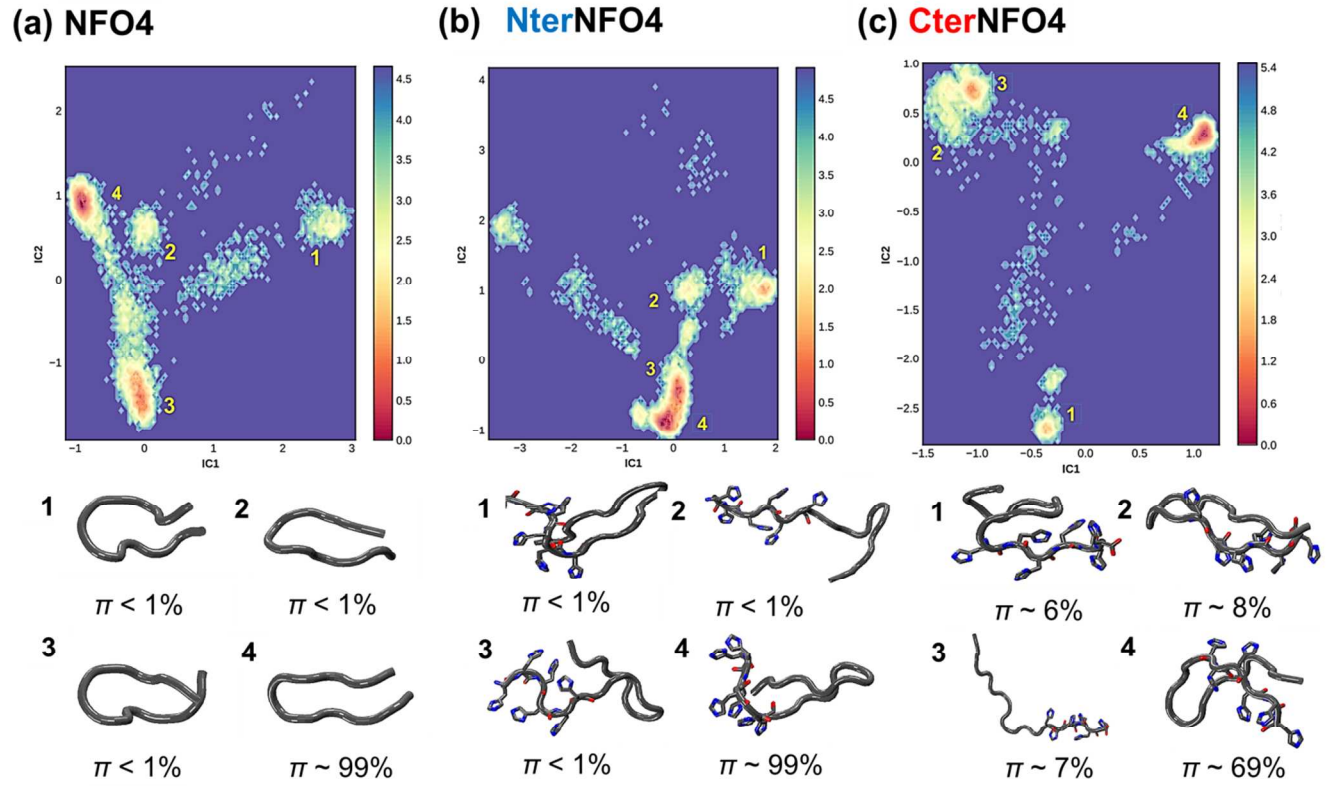


**Figure 2.** Illustration of the free energy landscape, the representative peptide configurations for each macrostate, and the equilibrium distributions associated with (A) NFO4, (B) NterNFO4, and (C) CterNFO4 as identified from MSM analysis of the trajectories obtained in BEMD accelerated sampling simulations. IC1 (x-axis) and IC2 (y-axis) represent the dimensional projection along the

top two components of the IC analysis. Peptide conformations corresponding to the four low free energy basins were identified as '1', '2', '3', and '4', and its equilibrium population distribution were designated as '$\pi$'. $\pi < 1\%$ were considered statistically insignificant peptide conformations. The scale bar indicates the free energy surface (FES, units of $k_bT$) associated with the peptide folding, with blue (higher number) indicating the least favorable configuration and red (lower number) indicating the most favorable configuration. Peptide segment similar toNFO4 were represented as *ribbons* (colored in grey), while the His residue side chains were displayed in *licorice* (colored by atom name).

**Site-Specific 6× His Tag Influenced the Hapten Binding Properties of the NFO4 Peptide.** Binding affinities and the equilibrium population distributions of the peptides bound to OTA and OTB were predicted using BEMD and MSM analysis. The FES associated with ochratoxin binding to the peptides are provided in Figure S7. The regions that are more intensely blue within the FES correspond to the less energetically favorable peptide-hapten configurations while the regions that were more intensely red correspond to the more energetically favorable configurations. The macrostates identified for each peptide-hapten configurations were represented by an individually colored marker. The placement of each colored marker within the FES represents the microstates from where the specific peptide-hapten configurations were sampled. For this study, peptides were considered bound to the haptens when the haptens were within 0.5 nm of the peptide. Based on the peptide-hapten contacts, at least two macrostates representing the bound and unbound states of the peptide were identified. The most populated bound and unbound states are shown in Figure 3. Table 2 summarizes the structural and thermodynamic preferences for the untagged and tagged NFO4 when bound to OTA and OTB. For each of the discrete macrostates identified from the FES maps, residue flexibility (Figures S8 and S9), water density surrounding the complex (Figures S10–S15), secondary structure preference (Figures S16 and S17), peptide-hapten contact maps (Figures S18 and S19), H-bonding profiles (Figures S20 and S21), energetic contribution to peptide-hapten binding (Tables S1-S2), and residue-level energetic breakup (Tables S3-S5) were evaluated to better understand the molecular-level processes involved in peptide binding to ochratoxins. As the binding energy estimates determined in this study were based on the definition provided in equation (1), most of the ensuing discussion is limited to the structural and energetic characteristics of the most dominant states.

**(a) Site-Specific 6× His Tag Significantly Influenced the Native Peptide's Interaction with OTA.** Figures 3a, 3c and 3e represent the most dominant equilibrium distributions of NFO4, NterNFO4 and CterNFO4 when bound and unbound to OTA, respectively. Table S1 provides an overview of the energetic breakdown for the peptide interactions with OTA, and Tables S3a, S4a, and S5a provide a residue-level energetic breakdown for peptide-OTA interaction. The combined data suggests that the presence of the tag significantly influenced the predicted in-solution binding affinities of the peptide to OTA.

Previous studies using experimental and simulation techniques had established that NFO4 binds with high affinity and selectivity to OTA.[34] In line with these results, NFO4 shows higher affinity and selectivity to OTA. Three macrostates were identified in NFO4-OTA system (Figure S7a): NFO4-OTA-'1' represented the unbound state of the peptide and NFO4-OTA-'0' and NFO4-OTA-'2' represented the bound state of the peptide-hapten complex. The bound configurations represented by the NFO4-OTA-'2' were energetically favored ($\Delta$PMF $\approx$ -10.4 kcal/mol) and dominated (> 99%) the sampled configurations. The unbound NFO4 peptides were relatively ordered (33% β-turn, 67% Coil) (Figure S16a), with a dense water layer surrounding the peptide and OTA (Figure S11). However, post-binding to OTA, both the NFO4 and the OTA underwent desolvation (Figure S12) and broke most of its intrinsic internal contacts (Figures S16, S18, and S19) to form new contacts with OTA. Contact map indicates that at least seven of the 12 residues (2-4, 6-8, and 10) were within 0.35 nm of OTA, among which at least three of the contacts were likely mediated via H-bonding. The disruption in the peptide's internal contacts resulted in a loss of its secondary structure. The loss in internal contacts, however, did not increase the average fluctuations of the individual residues but rather decreased them, probably due to the tight interactions between the residues in the peptide and OTA. Consistent with our previous reports, the higher affinity and selectivity of NFO4 to OTA stems from the lower solvation penalty associated with the NFO4-OTA complex.[32]

The addition of 6x His-tags at the N-terminus generally preserved the affinity and selectivity of NFO4 to OTA (Table 2). Two distinct macrostates (Figure. S7c) were identified:- NterNFO4-OTA-'0' (16% of the sampled conformations) and NterNFO4-OTA-'1' (84% of the sampled conformations) which represented the unbound and the bound states of the peptide respectively (Figure 3c). Among these two states, the bound state was energetically favored ($\Delta$PMF $\approx$ -9.8 kcal/mol). The addition of affinity tags at the N-terminus of NFO4 reduced the number of water molecules surrounding the peptide. But the NterNFO4 peptide interaction with OTA, induced more extensive desolvation in the hapten than the peptide (Figure S11). The peptide interaction with OTA disrupted many of the native contacts within the peptide (Figure. S18.b) to form new intra-molecular and peptide-hapten contacts (Figure. S20.b) all of which disrupted the peptide's ordered structure. Within the bound complex, OTA was found to be in contact with 12 of the 18 residues (residue numbers 2-6, 8, 11, 13-17) of which at least four of the contacts were mediated by H-bond interaction (Figure S19b). The intra-molecular and the peptide-hapten contacts were additionally responsible for the lowered residue fluctuations within the bound complex. In fact, the extensive increase in the non-bonded interactions with OTA was accompanied by an increase in the solvation penalty of NterNFO4-OTA complex. Despite the increase in solvation penalty for NterNFO4-OTA complex, the favorable interaction of histidine residues at the N-terminus with OTA (Table S4a), was the primary factor responsible for preserving the binding preference of the native peptide.

The addition of 6x His-tags at the C-terminus radically altered the binding behavior of the peptide, by effectively eliminating the native peptide's affinity and selectivity to OTA. Unlike other peptide systems, the peptide configurations corresponding to the unbound state (75%) were sampled more than the bound state (Figure 3e). The remaining configurations

represented the bound configurations, with CterNFO4-OTA-'2' representing the dominant configuration (Figure S7e). Both the unbound and bound states were sampled from the redder regions of the FES, with the bound state being slightly more energetically favored than the unbound state (ΔPMF ≈ -2.0 kcal/mol). When the Cter NFO4 were bound to OTA, the peptide and OTA underwent desolvation with the hapten desolvation being more prominent than the peptide desolvation. Also, the OTA interaction did not induce any significant secondary structural shift or significantly alter the native internal network within the peptide. At least one of the contacts between the CterNFO4 (residue numbers 5 and 6) and OTA was likely mediated via H-bond interaction. However, the contribution of non-bonded interaction within the CterNFO4-OTA system to the overall binding energetics was the least among all the OTA systems (Table S1). The residue-level assessment of the binding energetics, further indicated that the 6x His-tag in the CterNFO4 barely interacted with OTA. The positioning of the 6x His-tags significantly influenced the non-bonded contribution to the overall binding energetics (compare Tables S4a and Table S5a).

**(b) Site-Specific 6× His Tag Did Not Significantly Influence the Native Peptide's Interaction with OTB:** Figures 3b, 3d and 3f represent the most dominant equilibrium distributions of NFO4, NterNFO4 and CterNFO4 when bound and unbound to OTB, respectively. In general, diverse and broader distributions of conformational states were identified in the peptide interaction with-OTB system (Figures 3b, 3d, and 3f) as opposed to the peptide's interaction with OTA. Table S2 provide an overview of the energetic breakdown for the peptide interactions with OTB, and Tables S3b, S4b, and S5b provide a residue-level energetic breakdown for peptide-OTB interaction. As evident, the combined data suggests that the tagging process did not significantly affect the predicted in-solution affinities to OTB.

Similar to OTA, the binding interaction of NFO4 with OTB also involved desolvation of the peptide and OTB (Figures S13b-S15b), and disruption in the peptide's inherent contacts (Figures S17, S19, and S21) to form new contacts with OTB. The loss in intrinsic contacts compromised the 2° structural integrity of the NFO4 peptide, and was expected to increase the residue fluctuation. However, the increase in residue fluc tuation was primarily limited to the terminals of the peptide, with the other segments of the NFO4 peptide remaining rela tively intact. A probable reason for the lack in residue fluctua tion could be due to the new contacts formed between the res idues 3 9 in NFO4 and OTB. Of these new contacts, at least three contacts were mediated via H bonding. As it could be seen from the Tables S1 and S2, NFO4 shows a higher *in-solution* affinity and selectivity to OTA than OTB, despite the non bonded contributions for both systems being similar.

The addition of 6x His tags at the N terminal end of NFO4 (Figure 3d) also involved the formation of new peptide hapten contacts via the desolvation of the peptide and the hapten, and the disruption in the native contact network (Figures S14 and S19b). Although the disruption in the native contact network induced a loss in ordered secondary structure, the residue flex ibility in the bound state was lower than the unbound state, probably due to the peptide hapten contacts and the more ex tensive intra molecular contact network (Figures S17b, S19b, and S21b). The desolvation process however, promoted the non bonded interactions with OTB while increasing the solva tion penalty associated with the NterNFO4 OTB system.

In case of the CterNFO4 OTB system (Figure 3f), the desolvation process was accompanied by less extensive pep tide hapten contacts (Figures S14, S16c, and S18c). Further more, the relatively minor change in the internal contacts did not change the secondary structure of the peptide or alter the flexibility of the residues. In fact, the contribution of non bonded interaction and the solvation penalty within the CterNFO4 OTB system to the overall binding energetics was the least among all the OTB systems. (Tables S1 and S2). The residue level assessment of the binding energetics, further indicated that the 6x His tag in the CterNFO4 barely interact ed with OTB.

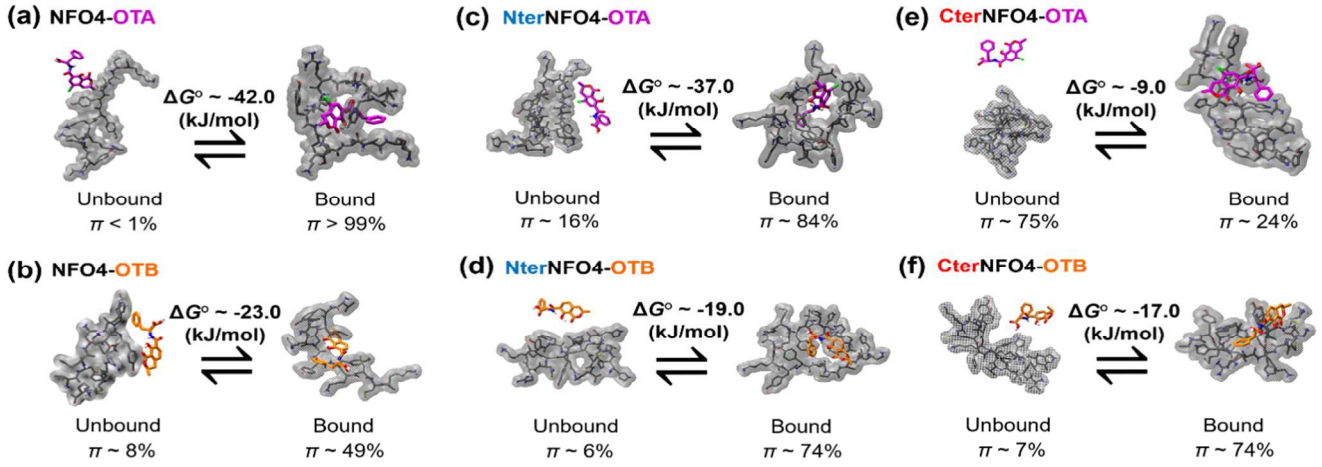


**Figure 3.** The representative states for unbound and bound peptide, equilibrium probabilities of these states (π), and free energies of binding (designated as ΔG° (kJ/mol)) (a) NFO-OTA, (b) NFO4-OTB, (c) NterNFO4-OTA, (d) NterNFO4-OTB, (e) CterNFO4-OTA, and (f) CterNFO4-OTB, identified from MSM analysis of the trajectories generated in BEMD enhanced sampling. 'π' represent the distribution of the most populated bound or unbound macrostates (the sums of probabilities of all bound, $p_{bound}$, and all un-

bound states, $p_{unbound}$, were used for binding free energy calculations in Equation 1). Peptides were depicted with the translucent *molecular surface* (in grey) and the ochratoxins were shown in *licorice* (colored by the default atom color except for carbon which was colored as magenta (for OTA) and orange (OTB)).

**Table 2. Structural and thermodynamic characteristics of the peptide-hapten complex**

| Recognition Molecule | Complex Dist.[1] (%) | Str. Shifs[2] | Cont. Freq.[3] | RMSF Shift[4] | $\Delta G^\circ$ (kJ/mol)[5] |
|---|---|---|---|---|---|
| NFO4-OTA | > 99 | Yes | 7/12 | Decreased | -42.34 (6.2) |
| NFO4-OTB | > 99 | Yes | 6/12 | Increased | -22.76 (5.52) |
| NterNFO4-OTA | ~84 | Yes | 12/18 | Decreased | -36.92 (7.92) |
| NterNFO4-OTB | ~94 | Yes | 6/18 | Decreased | -19.07 (1.69) |
| CterNFO4-OTA | ~25 | No | 2/18 | Decreased | -9.16 (2.42) |
| CterNFO4-OTB | ~93 | Yes | 5/18 | Decreased | -17.74 (2.34) |

[1] Complex Dist. refers to the overall bound fraction (%) of the peptide-hapten complex.
[2] Str. Shifts refers to the secondary structure shifts within the Pref. State relative to the unbound macrostate.
[3] Cont. Freq. refers to the average number of residues within 0.35 nm of the hapten within the Pref. Macro.
[4] RMSF Shift refers to the structural fluctuation within the Pref. State relative to the unbound macrostate.
[5] $\Delta G^\circ$ refers to the average equilibrium binding free energy. The values in the parenthesis provides the statistical error associated with $\Delta G^\circ$ estimates by block averaging the data over 20 ns.

**Validation of Results and Implications for Computer-Aided Design of Sensing Elements.** Table 3 compares the simulated *in-solution* affinity and selectivity with the immobilized state binding properties of the tagged and untagged peptides Previous studies using experimental and simulation techniques have established that NFO4 binds with high affinity and selectivity to OTA.[34] In line with these results, NFO4 showed higher affinity and selectivity to OTA than OTB. Though at least three different structural variants of ochratoxin are known to naturally occur, only OTA and OTB are found prevalently in food, feed and beverages.[3, 4] Of these two ochratoxins, OTA is more toxic [3] and has been known to bioaccumulate in the consumer, necessitating strict regulatory oversight. [3, 4, 51, 52] In this regard, biosensing platforms based on immobilized 6x His-tag conjugated NFO4 provide a cost-effective alternative to antibody based bioassays for the immunocapture of OTA in the detection and monitoring of OTA over OTB. But, a main challenge in the design of biosensing elements for OTA pertains to the selection and location of affinity tags, so as not to compromise the inherent activity of the molecular recognition entity. The choice of tag is particularly more challenging when the tags and sensing elements are of comparable size and chemistry.

In the current study, only the *in-solution* affinities of the 6× His tagged NFO4 were assessed. Our study indicated that the addition of affinity tags at either ends of the NFO4 favored solvation more than the untagged peptide Also, OTB is more hydrophilic than OTA and the improved solvation from the affinity tag placement at either ends of the peptide minimized the peptide interaction with OTB (Tables S1 and S2). The site of 6x His-tag placement influenced the native fold, with the tags at the Nter preserving the native fold and those at the Cter altering the fold. The alteration in the fold further affected the NFO4's interactions with OTA, with the NterNFO4 retaining the general affinity and selectivity to OTA while the CterNFO4 lacking any ochratoxin-specific recognition capabilities (by comparing the $\Delta G^\circ_{binding}$ in Table 2). Infact, among the tagged peptides, the affinities of NFO4 and NterNFO4 towards OTA were not significantly different but the affinity of CterNFO4 was ~4x lower than that of the native peptides. In a recent experimental study, involving the immobilization of 6× His tagged NFO4, Soleri et al. had demonstrated that the dense layers of immobilized NFO4 peptides were significantly better(2x) at OTA recognition when oriented on $Zn^{++}$-laden chitosan foams via N-terminus modification as opposed to C-terminus modification.[7, 8] While it is certainly encouraging to observe that the *in-solution* predictions from simulations generally followed the experimental data on immobilized system, a direct comparison of these results is challenging. For example, experimental studies on the immobilized hexamer (SNLHPK) on a wide range of substrates indicate that the peptide's affinity to OTA on solid phase ($K_D$ ~ 0.01 μM – 1.00 μM) were drastically different from those *in-solution* ($K_D$ ~ 29 μM).[53, 54] These observed differences in affinity would suggest that in addition to the molecular recognition entity, the surface may also have an active role in the hapten recognition, even though the exact mechanisms are currently unknown. Future studies could also explore and validate strategies that would minimize the direct interaction between the peptide and the tags by introducing more flexible spacers like polyethylene glycol (PEG) so as to assess if such modification could recover the native binding properties of the NFO4 irrespective of the site of modification. Nevertheless, the results presented in this study are in line with those and other studies that demonstrated the negative impact of 6x His tags on the binding properties of peptides especially when the tags were placed at the C-terminus of peptides/proteins.[18, 20, 22, 55] Based on these rationale, the current simulations were considered representative of the real-world binding interactions within an affinity tagged NFO4.

**Table 3. Binding properties (mean ±95% C.I.) of synthetic peptides to ochratoxins in a wine-like solution pH.**

| Recognition Molecule | $\Delta G°_{OTA\text{-}PRE}$ (kJ/mol) | $\Delta G°_{OTB\text{-}PRE}$ (kJ/mol) | $K_{D\text{-}OTA}$(μM) Pred. [1] | Selectivity Pred. [2] | Comments |
|---|---|---|---|---|---|
| NFO4 | -42.3 (6.2) | -22.8 (5.5) | 0.038 | ~1.9 | Immobilized NFO4 - 3x more selective to OTA than OTB [3] |
| NterNFO4 | -36.9 (7.9) | -19.1 (1.7) | 0.338 | ~1.9 | Immobilized NterNFO4 were 2.5x more effective at OTA detection than CterNFO4[4] |
| CterNFO4 | -9.2 (2.4) | -17.7 (2.3) | 24353 | ~0.5 | |

[1] The dissociation constant ($K_D$) for ochratoxins was estimated from the average $\Delta G°$ estimate using the equation $K_D = \frac{1}{\exp(-\frac{\Delta G}{RT})}$ where R = 0.00831 kJ mol$^{-1}$ K$^{-1}$and T = 298 K.
[2] Selectivity-Pred was based on the relative ratios of $\Delta G°_{OTA\text{-}PRE}$ to $\Delta G°_{OTB\text{-}PRE}$
[3] See Ref 6 Estimate using HPLC-FLD.
[4] See Ref 8 Estimate using fluorescence.

## CONCLUSIONS

Advanced sampling and MSM were used to assess the impact of site-specific 6x His tags on the *in-solution* binding properties of NFO4 to ochratoxins in a wine-like matrix environment. The *in-silico* framework outlined in the current study facilitated structural and thermodynamic characterization of the sensing elements with tags of comparable size and chemistry in detail that were otherwise not obtainable using routine experimental biophysics techniques or regular MD simulations. Results showed that the 6x His tag placement influenced the folding and binding behavior of the peptides. While the 6x His tags placed on the N-terminus of the NFO4 generally preserved the native fold of the peptide the tags altered the intrinsic contact network and actively interacted with OTA. The overall affinity and selectivity of NterNFO4 was driven by the combined influence of the non-bonded interactions involving OTA with the His residues and the higher solvation penalty of peptide-OTA complex. In contrast, the 6x His tags placed on the C-terminus of the NFO4 improved the stability of the native peptide by altering the native fold and the intrinsic contact network within the peptide. These His residues did not contribute significantly to the overall non-bonded energetics, and also introduced a higher solvation penalty for solvating the peptide-OTA complex as opposed to peptide-OTB complex. The non-bonded interactions and the solvation penalties associated with the NFO4 interaction with OTB were relatively unaffected by the site-specific placement of the tags. Consequently, the NterNFO4 preserved the generally affinity and selectivity of NFO4 while the CterNFO4 eliminated the OTA-specific binding capabilities of NFO4. However, the binding mechanisms of the NFO4 and NterNFO4 to OTA were different. The OTA-specific binding behavior of NFO4 was entirely driven by the lower solvation penalty of the NFO4-OTA, as opposed the OTA-specific binding by NterNFO4 that was driven by the interplay of non-bonded interactions and solvation penalty associated with the peptide-OTA complex.

While further work is certainly needed before the *in-silico* platforms presented in the current study could be reliably used to engineer peptides or direct peptide modifications with desired sensing efficacies to a target hapten, the mechanistic insights gained from the approach presented in this work can facilitate the selection and placement of affinity tags or the modification of the molecular recognition entity at least in a solution environment. In a broader sense, the methods outlined in the current study can be extended to virtually any peptide-based system so as to assess the impact of tags or site-specific tags on the peptide's intrinsic activity.

## ASSOCIATED CONTENT

The following supplementary materials are available online. **Figure S1:** Convergence plot in peptide folding simulation. **Figure S2:** Implied time scale plot of the folded peptide for (a) NFO4, (b) NterNFO4, and (c) CterNFO4, **Figure S3:** RMSF of the folded peptide. **Figure S4:** Secondary structural preferences of the folded peptides, **Figure S5:** Contact map of the folded peptides, **Figure S6:** Average H-bond profile in folded peptides. **Figure S7:** FES map of the peptide systems involved in ochratoxin binding. **Figure S8-S9:** RMSF of the peptide bound to OTA and OTB. **Figure S10-S12:** RDF of the peptides and OTA. **Figure S13-S15:** RDF of the peptides and OTB. **Figure S16-S17**: Secondary structural preferences of the peptides when bound to OTA and OTB. **Figure S18-S19**: Contact map of the residues within a peptide-hapten complex. **Figure S20-S21:** H-bond profile within the peptide-hapten complex. **Tables S1-S2:** Breakdown of the energetic components contributing to the overall binding energetics. **Tables S3-S5:** Residue-level contribution the overall binding energetics of each peptide system.

## AUTHOR INFORMATION


### Corresponding Author

*Anthony Guiseppi-Elie.
E-mail: guiseppi@tamu.edu. Phone: +1(979) 458 1239. Fax: +1(979) 458 8219.

### ORCID

Aby A. Thyparambil: 0000-0003-1760-1454
Tigran M. Abramyan: 0000-0002-7224-6072
Ingrid Bazin: 0000-0002-8293-5592
Anthony Guiseppi-Elie: 0000-0003-3218-9285


### Author Contributions

AG-E and AAT designed the study, AAT and TMA executed the study, TMA and IB contributed insights to the study, and AAT and AG-E wrote the manuscript.

### Notes

The authors declare no competing financial interest.

## ACKNOWLEDGMENT


The authors acknowledge the support of the computing and storage facility of Texas A & M University's High Performance Research Computing Resources.

## REFERENCES


1. Singh, M. K.; Srivastava, S.; Raghava, G. P.; Varshney, G. C., HaptenDB: A Comprehensive Database of Haptens, Carrier Proteins and Anti-hapten Antibodies. *Bioinformatics* **2006,** 22, (2), 253-5.
2. Erkes, D. A.; Selvan, S. R., Hapten-Induced Contact Hypersensitivity, Autoimmune Reactions, and Tumor Regression: Plausibility of Mediating Antitumor Immunity. *J Immunol Res* **2014,** 2014, 175265.
3. Malir, F.; Ostry, V.; Pfohl-Leszkowicz, A.; Malir, J.; Toman, J., Ochratoxin A: 50 Years of Research. *Toxins (Basel)* **2016,** 8, (7), 191.
4. Heussner, A. H.; Bingle, L. E., Comparative Ochratoxin Toxicity: A Review of the Available Data. *Toxins (Basel)* **2015,** 7, (10), 4253-82.
5. Ha, T. H., Recent Advances for the Detection of Ochratoxin A. *Toxins (Basel)* **2015,** 7, (12), 5276-300.
6. Bazin, I.; Tria, S. A.; Hayat, A.; Marty, J. L., New Biorecognition Molecules in Biosensors for the Detection of Toxins. *Biosens Bioelectron* **2017,** 87, 285-298.
7. Tria, S. A.; Lopez-Ferber, D.; Gonzalez, C.; Bazin, I.; Guiseppi-Elie, A., Microfabricated Biosensor for the Simultaneous Amperometric and Luminescence Detection and Monitoring of Ochratoxin A. *Biosens Bioelectron* **2016,** 79, 835-42.
8. Soleri, R.; Demey, H.; Tria, S. A.; Guiseppi-Elie, A.; Hassine, A. I.; Gonzalez, C.; Bazin, I., Peptide Conjugated Chitosan Foam as a Novel Approach for Capture-Purification and Rapid Detection of Hapten--Example of Ochratoxin A. *Biosens Bioelectron* **2015,** 67, 634-41.
9. Goldman, E. R.; Cohill, T. J.; Patterson, C. H.; Anderson, G. P.; Kusterbeck, A. W.; Mauro, J. M., Detection of 2,4,6-Trinitrotoluene in Environmental Samples Using a Homogeneous Fluoroimmunoassay. *Environmental Science & Technology* **2003,** 37, (20), 4733-4736.
10. Bade, S.; Rockendorf, N.; Franek, M.; Gorris, H. H.; Lindner, B.; Olivier, V.; Schaper, K. J.; Frey, A., Biolabeling with 2,4-dichlorophenoxyacetic acid derivatives: the 2,4-D tag. *Anal Chem* **2009,** 81, (23), 9695-702.
11. Grieshaber, D.; MacKenzie, R.; Voros, J.; Reimhult, E., Electrochemical Biosensors - Sensor Principles and Architectures. *Sensors (Basel)* **2008,** 8, (3), 1400-1458.
12. Madrid, R. E.; Chehín, R.; Chen, T.-H.; Guiseppi-Elie, A., Biosensors and Nanobiosensors. In *Further Understanding of the Human Machine: The Road to Bioengineering*, Valentinuzzi, M. E., Ed. World Scientific Publishing Co.: Singapore, 2017.
13. Arnau, J.; Lauritzen, C.; Petersen, G. E.; Pedersen, J., Reprint of: Current Strategies for the Use of Affinity Tags and Tag Removal for the Purification of Recombinant Proteins. *Protein Expr Purif* **2011**.
14. Kimple, M. E.; Brill, A. L.; Pasker, R. L., Overview of Affinity Tags for Protein Purification. In *Current Protocols in Protein Science*, John Wiley & Sons, Inc.: 2001.
15. Bornhorst, J. A.; Falke, J. J., Purification of Proteins using Polyhistidine Affinity Tags. *Methods in Enzymology* **2000,** 326, 245-254.
16. Kang, E.; Park, J. W.; McClellan, S. J.; Kim, J. M.; Holland, D. P.; Lee, G. U.; Franses, E. I.; Park, K.; Thompson, D. H., Specific Adsorption of Histidine-Tagged Proteins on Silica Surfaces Modified with Ni2+/NTA-Derivatized Poly(ethylene glycol). *Langmuir* **2007,** 23, (11), 6281-8.
17. Samanta, D.; Sarkar, A., Immobilization of Bio-Macromolecules on Self-Assembled Monolayers: Methods and Sensor Applications. *Chem Soc Rev* **2011,** 40, (5), 2567-92.
18. Goel, A.; Colcher, D.; Koo, J. S.; Booth, B. J.; Pavlinkova, G.; Batra, S. K., Relative Position of the Hexahistidine Tag Effects Binding Properties of a Tumor-Associated Single-Chain Fv Construct. *Biochim Biophys Acta* **2000,** 1523, (1), 13-20.
19. Chant, A.; Kraemer-Pecore, C. M.; Watkin, R.; Kneale, G. G., Attachment of a Histidine Tag to the Minimal Zinc Finger Protein of the Aspergillus nidulans Gene Regulatory Protein AreA Causes a Conformational Change at the DNA-Binding Site. *Protein Expr Purif* **2005,** 39, (2), 152-9.
20. Carson, M.; Johnson, D. H.; McDonald, H.; Brouillette, C.; Delucas, L. J., His-Tag Impact on Structure. *Acta Crystallogr D Biol Crystallogr* **2007,** 63, (Pt 3), 295-301.
21. Panek, A.; Pietrow, O.; Filipkowski, P.; Synowiecki, J., Effects of the Polyhistidine Tag on Kinetics and Other Properties of Trehalose Synthase from *Deinococcus geothermalis*. *Acta Biochim Pol* **2013,** 60, (2), 163 6.
22. Majorek, K. A.; Kuhn, M. L.; Chruszcz, M.; Anderson, W. F.; Minor, W., Double Trouble-Buffer Selection and His-tag Presence may be Responsible for Nonreproducibility of Biomedical Experiments. *Protein Sci* **2014,** 23, (10), 1359-68.
23. Wang, X.; Campoli, M.; Ko, E.; Luo, W.; Ferrone, S., Enhancement of ScFv Fragment Reactivity with Target Antigens in Binding Assays following Mixing with Anti-tag Monoclonal Antibodies. *J Immunol Methods* **2004,** 294, (1-2), 23-35.
24. Strop, P.; Liu, S. H.; Dorywalska, M.; Delaria, K.; Dushin, R. G.; Tran, T. T.; Ho, W. H.; Farias, S.; Casas, M. G.; Abdiche, Y.; Zhou, D.; Chandrasekaran, R.; Samain, C.; Loo, C.; Rossi, A.; Rickert, M.; Krimm, S.; Wong, T.; Chin, S. M.; Yu, J.; Dilley, J.; Chaparro-Riggers, J.; Filzen, G. F.; O'Donnell, C. J.; Wang, F.; Myers, J. S.; Pons, J.; Shelton, D. L.; Rajpal, A., Location Matters: Site of Conjugation Modulates Stability and Pharmacokinetics of Antibody Drug Conjugates. *Chem Biol* **2013,** 20, (2), 161-7.
25. Plum, A.; Jensen, L. B.; Kristensen, J. B., *In vitro* Protein Binding of Liraglutide in Human Plasma Determined by Reiterated Stepwise Equilibrium Dialysis. *J Pharm Sci* **2013,** 102, (8), 2882-8.
26. Waters, N. J.; Jones, R.; Williams, G.; Sohal, B., Validation of a Rapid Equilibrium Dialysis Approach for the Measurement of Plasma Protein Binding. *J Pharm Sci* **2008,** 97, (10), 4586-95.
27. Naik, R. R.; Hagen, J. A.; Slocik, J. M.; Schmucker, A. L.; Singamaneni, S., Localized Surface Plasmon Resonance Sensing of Human Performance Biomarkers using Short Peptide Recognition Elements on Optically Active Metal Nanostructures. In Google Patents: 2017.
28. Karlsson, R.; Pol, E.; Frostell, A., Comparison of Surface Plasmon Resonance Binding Curves for Characterization of Protein Interactions and Analysis of Screening Data. *Anal Biochem* **2016,** 502, 53-63.
29. Oliveberg, M.; Wolynes, P. G., The Experimental Survey of Protein-Folding Energy Landscapes. *Q Rev Biophys* **2005,** 38, (3), 245-88.
30. Lane, T. J.; Shukla, D.; Beauchamp, K. A.; Pande, V. S., To Milliseconds and Beyond: Challenges in the Simulation of Protein Folding. *Curr Opin Struct Biol* **2013,** 23, (1), 58-65.
31. Boehr, D. D.; Nussinov, R.; Wright, P. E., The Role of Dynamic Conformational Ensembles in Biomolecular Recognition. *Nat Chem Biol* **2009,** 5, (11), 789-96.
32. Mobley, D. L.; Dill, K. A., Binding of Small-Molecule Ligands to Proteins: "What You See" is Not Always "What You Get". *Structure* **2009,** 17, (4), 489-98.
33. Plattner, N.; Noe, F., Protein Conformational Plasticity and Complex Ligand-Binding Kinetics Explored by Atomistic Simulations and Markov Models. *Nat Commun* **2015,** 6, 7653.
34. Thyparambil, A. A.; Bazin, I.; Guiseppi-Elie, A., Evaluation of Ochratoxin Recognition by Peptides Using Explicit Solvent Molecular Dynamics. *Toxins* **2017,** 9, (5), 164.
35. Bazin, I.; Andreotti, N.; Hassine, A. I.; De Waard, M.; Sabatier, J. M.; Gonzalez, C., Peptide binding to ochratoxin A mycotoxin: a new approach in conception of biosensors. *Biosens Bioelectron* **2013,** 40, (1), 240-6.
36. Cossio, P.; Trovato, A.; Pietrucci, F.; Seno, F.; Maritan, A.; Laio, A., Exploring the Universe of Protein Structures beyond the Protein Data Bank. *PLoS Comput. Biol.* **2010,** 6, (11), e1000957.
37. Doerr, S.; Harvey, M. J.; Noe, F.; De Fabritiis, G., HTMD: High-Throughput Molecular Dynamics for Molecular Discovery. *J Chem Theory Comput* **2016,** 12, (4), 1845-52.
38. Humphrey, W.; Dalke, A.; Schulten, K., VMD: Visual Molecular Dynamics. *J Mol Graph* **1996,** 14, (1), 33-8, 27-8.
39. Irwin, J. J.; Sterling, T.; Mysinger, M. M.; Bolstad, E. S.; Coleman, R. G., ZINC: A Free Tool to Discover Chemistry for Biology. *J Chem Inf Model* **2012,** 52, (7), 1757-68.
40. Koziara, K. B.; Stroet, M.; Malde, A. K.; Mark, A. E., Testing and Validation of the Automated Topology Builder (ATB) Version 2.0: Prediction of Hydration Free Enthalpies. *J Comput Aided Mol Des* **2014,** 28, (3), 221-33.
41. Abraham, M. J.; Murtola, T.; Schulz, R.; Páll, S.; Smith, J. C.; Hess, B.; Lindahl, E., GROMACS: High Performance Molecular Simulations through Multi-Level Parallelism from Laptops to Supercomputers. *SoftwareX* **2015,** 1-2, 19-25.
42. Wang, D.; Freitag, F.; Gattin, Z.; Haberkern, H.; Jaun, B.; Siwko, M.; Vyas, R.; van Gunsteren, W. F.; Dolenc, J., Validation of the

GROMOS 54A7 Force Field Regarding Mixed α/β□Peptide Molecules. *Helvetica Chimica Acta* **2012,** 95, (12), 2562-2577.
43. Huang, W.; Lin, Z.; van Gunsteren, W. F., Validation of the GROMOS 54A7 Force Field with Respect to beta-Peptide Folding. *J Chem Theory Comput* **2011,** 7, (5), 1237-43.
44. Cossio, P.; Marinelli, F.; Laio, A.; Pietrucci, F., Optimizing the Performance of Bias-Exchange Metadynamics: Folding a 48-residue LysM Domain using a Coarse-Grained Model. *J Phys Chem B* **2010,** 114, (9), 3259-65.
45. Pietrucci, F.; Marinelli, F.; Carloni, P.; Laio, A., Substrate Binding Mechanism of HIV-1 Protease from Explicit-Solvent Atomistic Simulations. *J Am Chem Soc* **2009,** 131, (33), 11811-8.
46. Bonomi, M.; Branduardi, D.; Bussi, G.; Camilloni, C.; Provasi, D.; Raiteri, P.; Donadio, D.; Marinelli, F.; Pietrucci, F.; Broglia, R. A.; Parrinello, M., PLUMED: A Portable Plugin for Free-Energy Calculations with Molecular Dynamics. *Computer Physics Communications* **2009,** 180, (10), 1961-1972.
47. Chodera, J. D.; Noe, F., Markov State Models of Biomolecular Conformational Dynamics. *Curr Opin Struct Biol* **2014,** 25, 135-44.
48. Pande, V. S.; Beauchamp, K.; Bowman, G. R., Everything You Wanted to Know about Markov State Models but were Afraid to Ask. *Methods* **2010,** 52, (1), 99-105.
49. McGibbon, R. T.; Beauchamp, K. A.; Harrigan, M. P.; Klein, C.; Swails, J. M.; Hernandez, C. X.; Schwantes, C. R.; Wang, L. P.; Lane, T. J.; Pande, V. S., MDTraj: A Modern Open Library for the Analysis of Molecular Dynamics Trajectories. *Biophys J* **2015,** 109, (8), 1528-32.
50. Kumari, R.; Kumar, R.; Open Source Drug Discovery, C.; Lynn, A., *g_mmpbsa*--A GROMACS Tool for High-Throughput MM-PBSA Calculations. *J Chem Inf Model* **2014,** 54, (7), 1951-62.
51. Malir, F.; Ostry, V.; Pfohl-Leszkowicz, A.; Novotna, E., Ochratoxin A: Developmental and Reproductive Toxicity-An Overview. *Birth Defects Res B Dev Reprod Toxicol* **2013,** 98, (6), 493-502.
52. Kőszegi, T.; Poór, M., Ochratoxin A: Molecular Interactions, Mechanisms of Toxicity and Prevention at the Molecular Level. *Toxins* **2016,** 8, (4), 111.
53. Giraudi, G.; Ferrero, V. E.; Anfossi, L.; Baggiani, C.; Giovannoli, C.; Tozzi, C., Solid-Phase Extraction of Ochratoxin A from Wine based on a Binding Hexapeptide Prepared by Combinatorial Synthesis. *J Chromatogr A* **2007,** 1175, (2), 174-80.
54. Giovannoli, C.; Passini, C.; Volpi, G.; Di Nardo, F.; Anfossi, L.; Baggiani, C., Peptide-Based Affinity Media for Solid-Phase Extraction of Ochratoxin A from Wine Samples: Effect of the Solid Support on Binding Properties. *Talanta* **2015,** 144, 496-501.
55. Thielges, M. C.; Chung, J. K.; Axup, J. Y.; Fayer, M. D., Influence of Histidine Tag Attachment on Picosecond Protein Dynamics. *Biochemistry* **2011,** 50, (25), 5799-805.

# NFO4-OTA

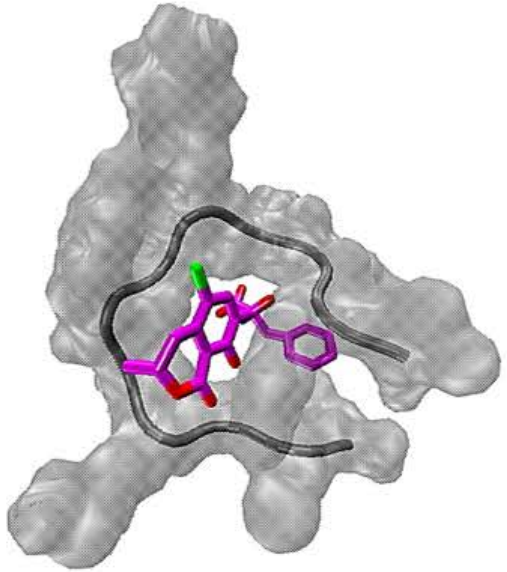

$K_D$ ~0.04 µM

Equil. pop. ~99%

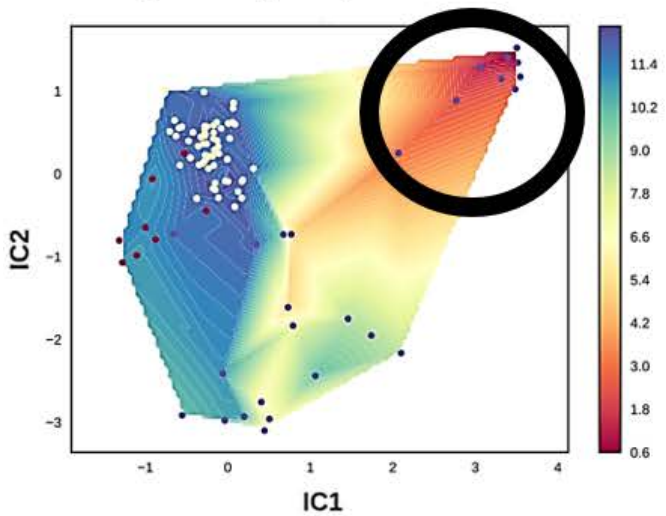


# NterNFO4-OTA

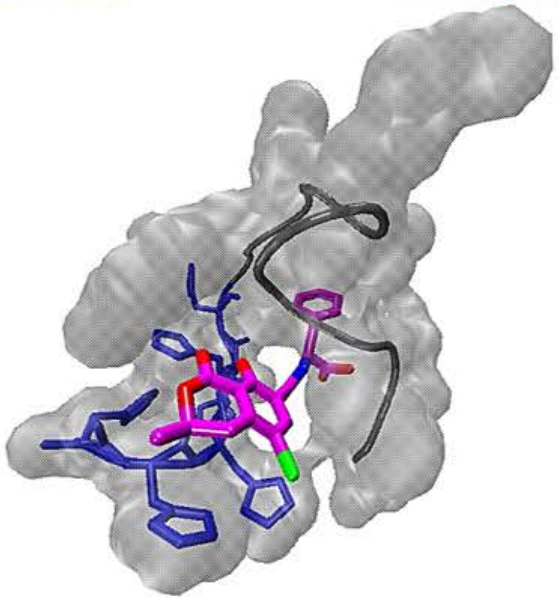

$K_D$ ~0.3 µM

Equil. pop. ~84%

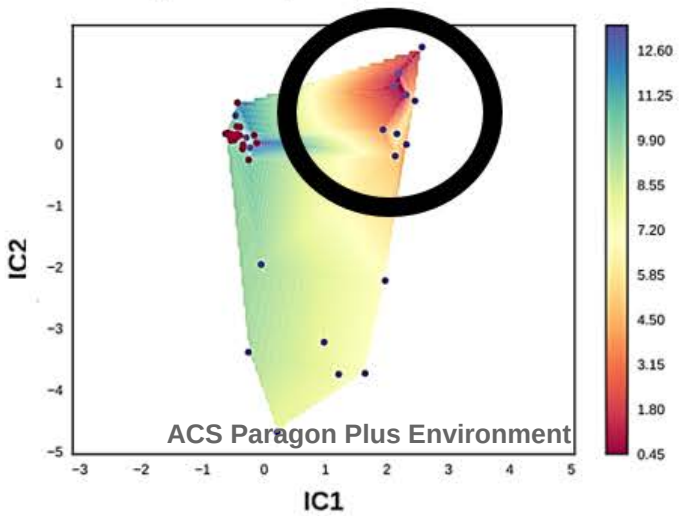


# CterNFO4-OTA

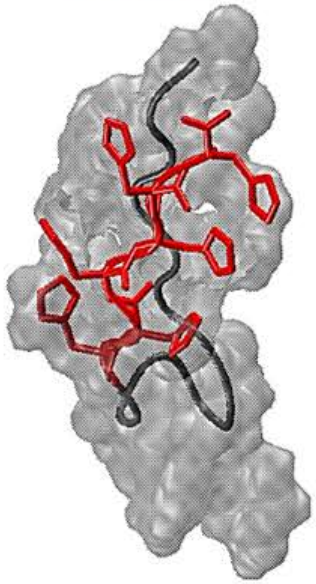

$K_D$ ~24,353 µM

Equil. pop. ~75%